EVALUATION OF THE OUTPUT FROM A BENT-

BEAM MEDICAL LINEAR ACCELERATOR

A Thesis

Submitted to the Graduate Faculty of the
Louisiana State University and
Agricultural and Mechanical College
in partial fulfillment of the
requirements for the degree of
Master of Science

in

The Department of Nuclear Engineering

by

Grayson Scott Young, Jr.
B.S., Louisiana State University, 1974

August, 1978

DEDICATED TO

My Mother and Father

ACKNOWLEDGMENT

The author would like to express his sincere appreciation to his major professor, Dr. Frank A. Iddings, for his assistance, encouragement, advice, understanding, and guidance during the preparation of this work.

The author is thankful to Dr. Edward N. Lambremont and Dr. Robert C. McIlhenny for their helpful advice, comments and encouragement.

A very special word of thanks is given to Mr. William Kubricht, Jr., the therapeutic radiological physicist at the Mary Bird Perkins Radiation Treatment Center in Baton Rouge, Louisiana for taking time out of his busy schedule to participate in this work. The author is most appreciative of his encouragement, interest and instruction.

The author wishes to thank the Board of Directors of the Mary Bird Perkins Radiation Treatment Center for allowing him to use their facilities and equipment for this work. The author also thanks the entire staff and management of the Mary Bird Perkins Radiation Treatment Center for their suggestions, friendliness and help.

The author wishes to thank Jack R. Little, Jr., for his enthusiasm and many helpful suggestions during the preparation of this work.

The author wishes to thank Prissy Milligan and Pam Davison for typing this thesis with the many revisions before the deadline.

TABLE OF CONTENTS

LIST OF FIGURES

ABSTRACT

The deceleration of high-energy electrons in the metal target of a linear accelerator produces high-energy photons for use in radiation therapy. Fast neutrons are produced during operation of a linear accelerator as a result of (γ,n) and $(e,e'n)$ reactions with various components of the accelerator. In this work the maximum neutron dose and neutron dose equivalent were determined at the isocentric position of a Varian Clinac-18 linear accelerator to be $5.4 \times 10^{-4}\%$ and $5 \times 10^{-3}\%$ of the photon dose respectively. The collimation (field-size) as well as the photon dose rate was found to have a pronounced effect upon these values. Prior to this publication the effects of collimation and photon dose rate on neutron production have not been adequately treated if indeed treated at all.

CHAPTER I

Introduction

The Varian Clinac-18 ® Linear Accelerator [1]

The Clinac-18 is an isocentric medical linear accelerator with a standing-wave accelerator guide structure approximately 1.4 meters long utilizing side-coupling cavities to create a resonant standing-wave oscillating with time (see Figure I-1, A and B). The standing-wave condition increases the electron acceleration per unit length compared to a traveling wave guide design and thereby minimizes power loss in the accelerator.

The assembly is mounted in a rotating gantry with a target-to-axis distance of 100 cm. The gantry contains an electron-beam-bending system and a collimating jaw system. The electron-beam-bending system which bends the beam 270 degrees and then downward from the horizontal is completely achromatic with appropriate energy—defining slits Figures I-1A(4) and I-1B(A and B).

The collimating-jaw system is composed of two pairs of tungsten collimators Figures I-1A(10) and I-1B(I and J) which move tangentially to the field of irradiation thus providing variable collimation. This system also contains a field-defining light and range-finder Figure I-1A(8 and 9) for accurate determination of the field-size at the depth of dose maximum and the target-to-skin distance. A redundant trans-mission ion chamber located above the collimators Figures I-1A(7) and I-1B(H) monitors the useful beam of radiation. This ion chamber has

Figure I-1A

Simplified Diagram of Clinac-18 Linear Accelerator
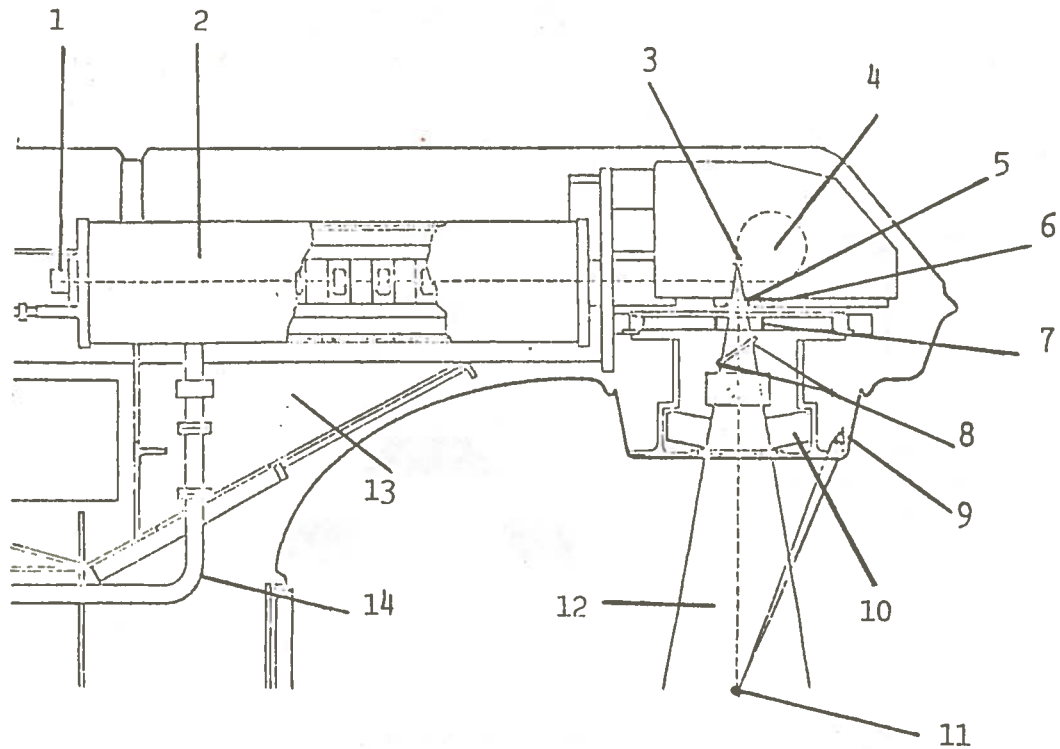
1. Gridded electron gun
2. Standing wave accelerator
3. Retractable copper target (photon mode only)
4. 270° bending electromagnet
5. Retractable flattening filter (photon mode only)
6. Scattering foils (electron beam mode only)
7. Full beam monitoring ion chamber
8. Field defining light
9. Optical range finder
10. Variable tungsten collimators
11. Isocenter
12. 10 MV x-rays; electrons 6, 9, 12, 15, 18 MeV.
13. Gantry
14. Wave guide
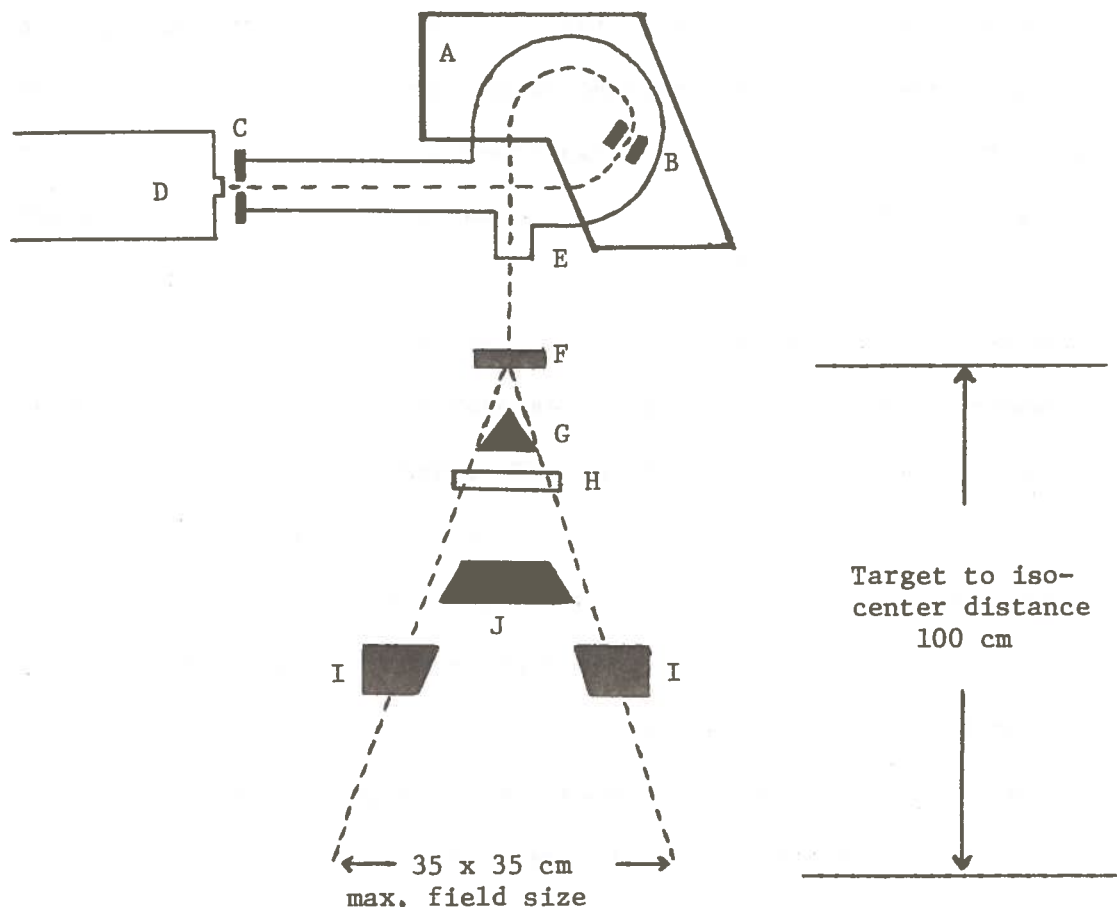
A. 270° bending electromagnet
B. Electron beam energy defining slit
C. Entrance slit
D. Exit of accelerator
E. Berylium thin end-window
F. Retractable copper target.
G. Flattening filter (photon mode); or appropriate scattering foil
H. Full beam monitoring ion chamber
I. Variable lower tungsten collimators
J. Variable upper tungsten collimators

Figure I-1B

Simplified Diagram of Clinac-18 Linear Accelerator

two plates for measuring integrated dose (extrapolated to 100 cm). A mechanism which positions the flattening filter for the photon mode of operation is located above the ion chamber. Scattering foils for the five electron energy settings (6, 9, 12, 15, and 18 MeV) in the electron mode of operation are also similarly located in Figures I-1A(5 and 6) and I-1B(F and G).

The accelerator is controlled from the operator's station located outside of the concrete-shielded treatment room for reasons of health physics and safety. The control console is transistorized and uses light-emitting diodes to indicate dose, time and pertinent treatment parameters. The control console allows selection of the treatment mode and electron-beam energy and also allows one to set the integrated dose to be delivered to the patient for a predetermined time. The console displays the status of the safety interlocks in the system. The safety interlocks automatically shut off the accelerator if any malfunctions occur in any of the subsystems comprising the interlock circuitry.
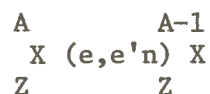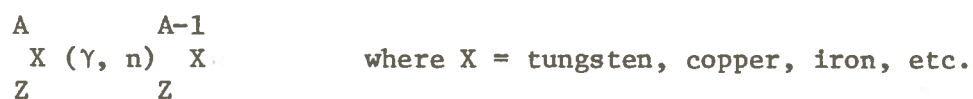
A motorized treatment couch is provided which can be moved in the x, y, and z axis. Rotation is also provided angularly about the vertical axis which also passes through the isocenter of gantry rotation.

Objective

The objective of this work is to evaluate the significance
of the total neutron contamination on the output of the Varian Clinac-18
linear accelerator.

Neutron Production, A Possibly Undesirable Component of the
Accelerator Beam

Neutrons are produced during the operation of a high-energy
linear accelerator which contaminate the radiation beam. These neutrons
result from high-energy photon and electron interactions with the
target, shield, collimator, flattening filter and other components
inside the accelerator.[2,3] The following generalized reactions can
produce neutrons.

$$\underset{Z}{\overset{A}{X}} (\gamma, n) \underset{Z}{\overset{A-1}{X}} \qquad \text{where X = tungsten, copper, iron, etc.}$$

$$\underset{Z}{\overset{A}{X}} (e,e'n) \underset{Z}{\overset{A-1}{X}}$$

The cross-sections for high-energy photoneutron production
or photodisintegration of many nuclides have been studied by investi-
gators and reported in the literature. [4,5]

The cross-sections to produce a neutron from a high-energy
electron interaction with a nucleus are lower by a factor of about
0.0025 than the cross-sections for photoneutron production.[2] The
accelerator current is considerably reduced in the electron beam mode
of operation as compared to the x-ray (10 MV photon) mode of operation.[6]

Thus, the greatest production of neutrons occurs during the x-ray mode of operation with a high dose rate [500 monitor units per minute where one monitor unit equals one rad at the depth for maximum dose, D_{max}] with the collimators closed.

CHAPTER II

EXPERIMENTAL PROCEDURES

Materials

1. Multichannel analyzer, 1024 channels, Tracor Northern Model TN-1705

2. Indium foils, 0.9537 gram and 0.9276 gram

3. Cadmium disks

4. 3" x 3" NaI(Tl) crystal, Harshaw type 12S

5. Portable neutron rem counter, Eberline model PNR-4 with tissue
   equivalent Bonner sphere (ball).

6. Shield, Clinac-4 accelerator room.

Methods

The gamma-spectroscopy counting system was set up inside the

Clinac-4 accelerator room (a different accelerator room than the one

in which the foils were activated) as shown in Figure II-1.

Two indium foils were activated. One foil was covered on top

and bottom by a disk of cadmium. Each foil was placed at the isocenter

on top of the treatment couch and activated with a total of 4,995

monitor units delivered with a dose rate of approximately 500 monitor

units min^{-1}.

The collimators were closed during the activation of these

foils. The activation time for each foil was approximately eleven

minutes. The collimators, which are composed of tungsten metal,

increased the production of neutrons by over four fold. This phenomena

occurred because the threshold for photoneutron production in tungsten

is near 7 MeV. This procedure also kept the photoactivation of the

Figure II-1

Diagram of Equipment Set-up for Neutron Foil Measurements

NaI (Tl) 3" x 3" crystal

Pmt

PREAMP

AMP

MCA

Hv

*
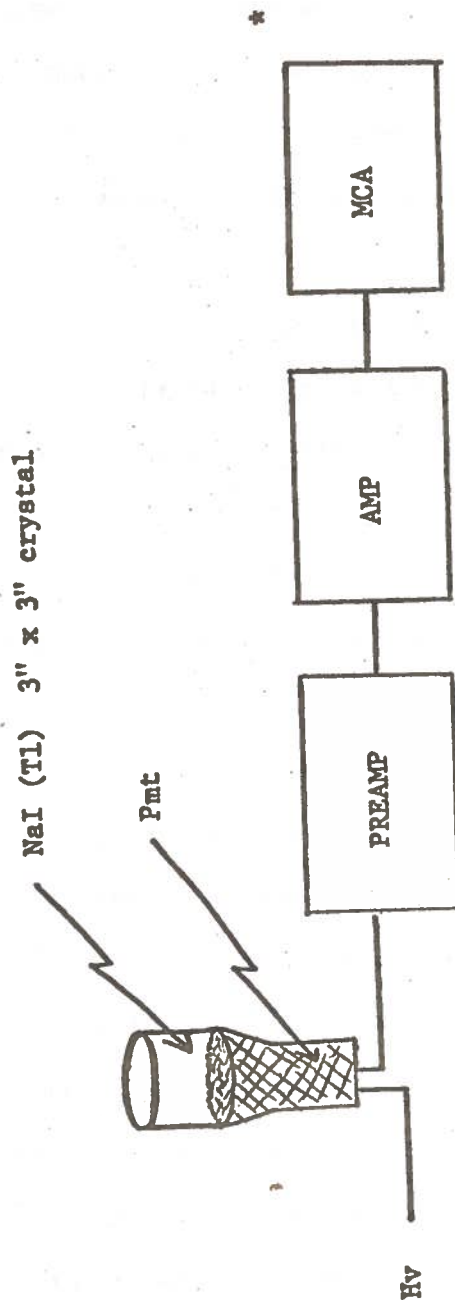
* No printer (data recorded from pulse-height integration function).

cadmium disks and indium foils to a minimum since the leakage of photons through the collimators is less than 0.5%. The activated foils were held for two minutes before counting to insure decay of any short half-lifed metastable states of indium-116. Each foil was counted for ten minutes. A ten minute background count was made at the end of the experiment.

The counting system was calibrated with cesium-137 and cobalt-60. An efficiency calibration was also done using a calibrated (National Bureau of Standards) cobalt-60 button source with an activity of 0.8696 µCi.

The thermal neutron flux and epithermal neutron flux were separately measured by indium foil activations. Appropriate conversion factors from the literature were applied to obtain neutron dose rates and neutron dose equivalent rates (see calculations section).

A neutron detector and tissue-equivalent Bonner ball was employed to measure directly the total dose equivalent rate produced by neutrons of all energies. This neutron-detection system is gamma insensitive and reads directly in mrem; it is sensitive to thermal, epithermal and fast neutrons. For this measurement, the Bonner ball was placed on the treatment couch with its center (the sensitive region of the detector) coincident with the isocenter. The collimators were closed and the accelerator was run at 500 monitor units min^{-1} in the 10 MV photon mode. A reading of 1500 mrem hr^{-1} was obtained. Another measurement was made with the same conditions with both collimators open with a 35 x 35 cm. field size. The dose equivalent rate was observed to drop to 350 mrem hr^{-1}.

A measurement was made to determine the dose-equivalent rate resulting from epithermal and fast neutrons. The PNR-4 detector was shielded from the thermal neutrons in the neutron flux by completely encasing the Bonner ball in a sheet of cadmium which was molded into a spherical shape. The exposure technique described previously was used for the cadmium-covered exposure. A reading of 1500 mrem hr^{-1} was obtained with the collimators closed and 350 mrem hr^{-1} was obtained when the collimators were open. These values, identical to those noted before, indicate no measurable contribution of thermal neutrons to the total neutron dose equivalent rate by this method.

Neutron production during operation of the Clinac-18 linac in the x-ray mode was observed to vary with collimator field size and accelerator dose rate. Measurements were made with the PNR-4 neutron detector and Bonner ball to investigate this relationship further. The Bonner ball was placed with its sensitive region coincident with the isocenter. The total neutron dose equivalent rate was determined for various square field sizes and photon dose rates. With each field size, the total neutron dose equivalent rate was observed to increase linearly as the photon dose rate was increased. The slope of the lines obtained by graphing the applied photon dose rate in rads min^{-1} versus the total neutron dose equivalent rate in mrem hr^{-1} was seen to increase as the collimators were closed. A maximum slope was obtained with the collimators closed (See Figures II-2&3).

The Bonner ball detector was housed in a metal case and connected to the hand-held survey meter (which was also housed in a
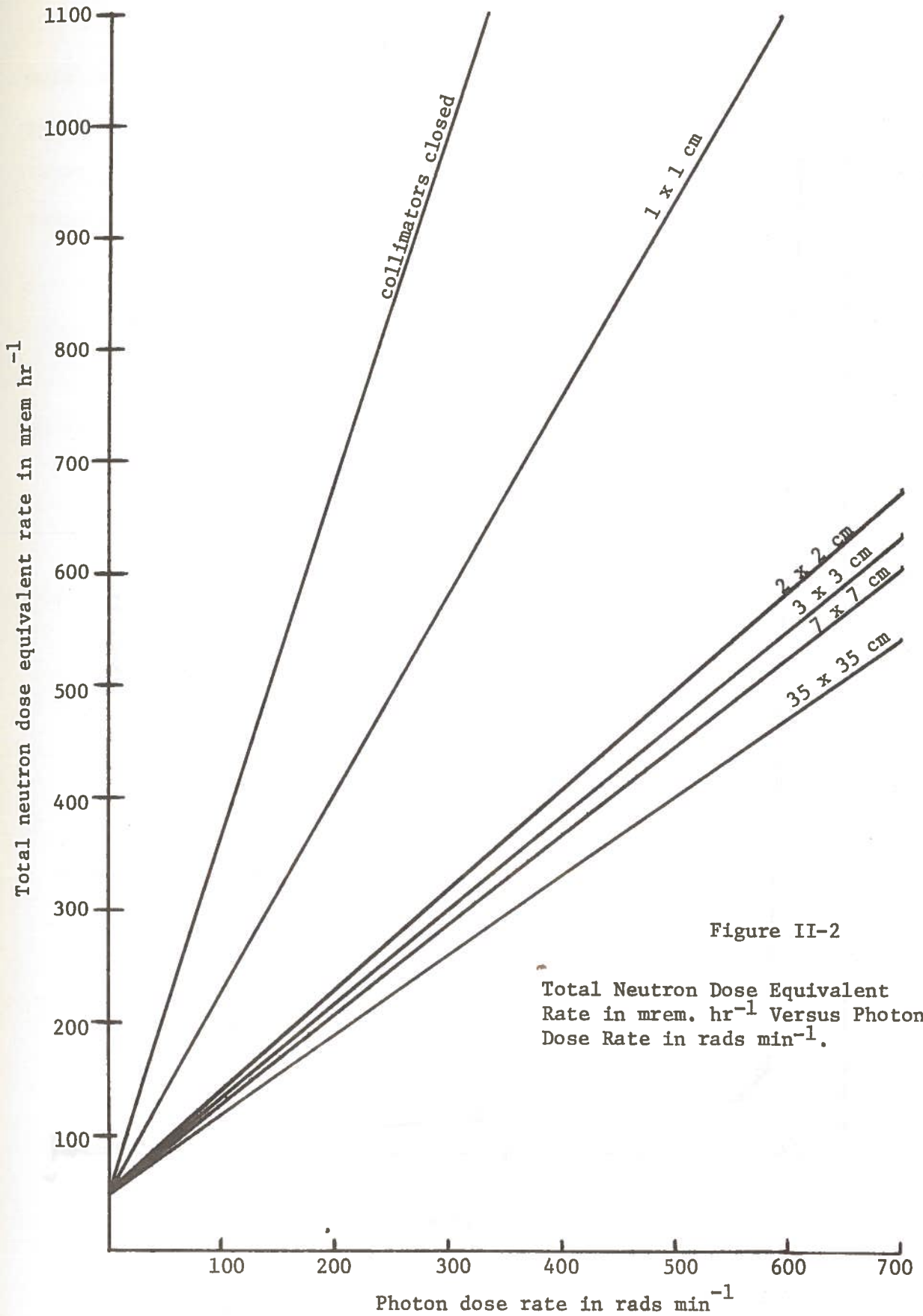
Figure II-2

Total Neutron Dose Equivalent
Rate in mrem. hr⁻¹ Versus Photon
Dose Rate in rads min⁻¹.

Figure II-3

Slope of lines from graph of photon dose rate in rads min^{-1} versus total neutron dose equivalent rate in mrem hr^{-1} plotted as a function of collimation (field size)
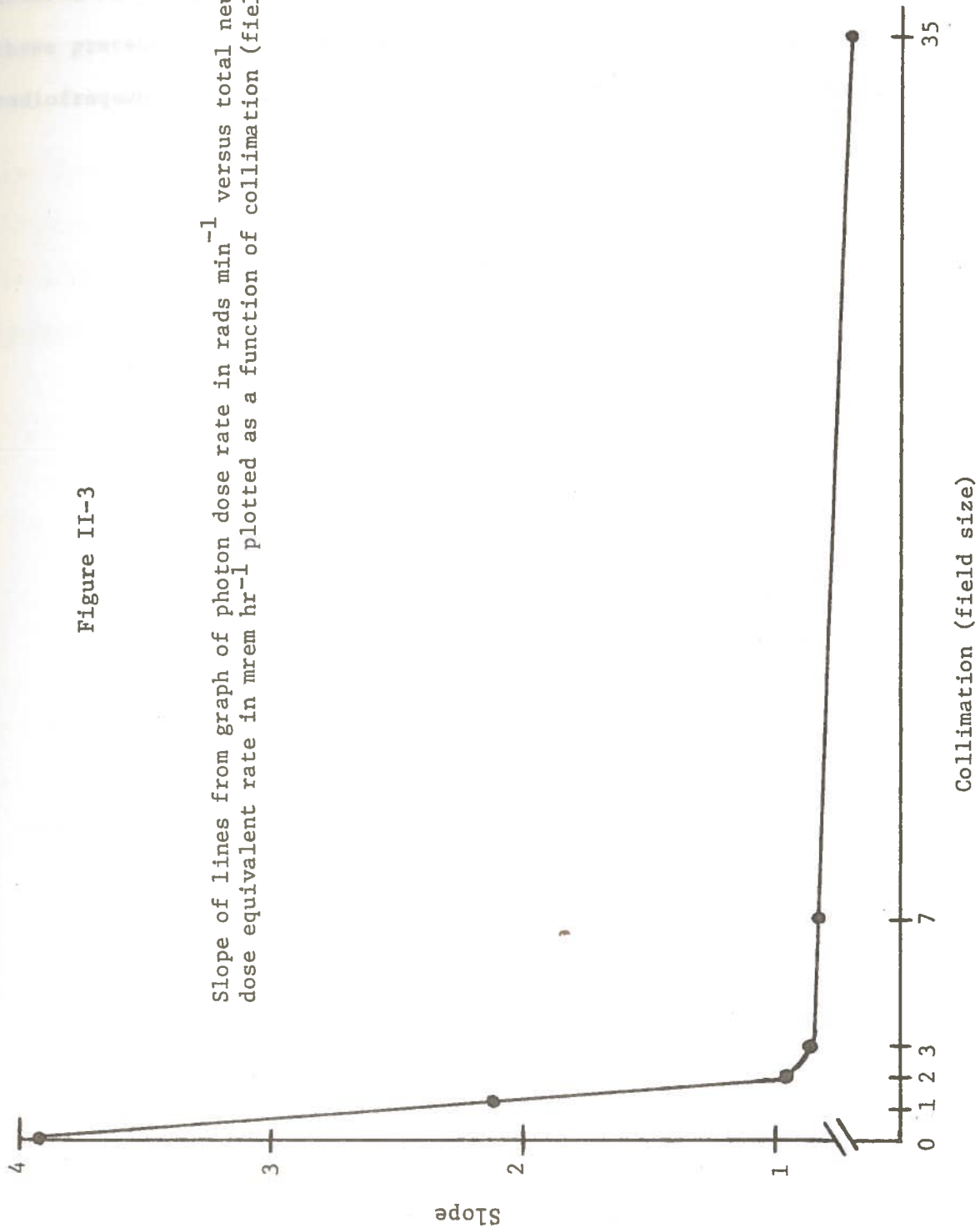
metal case) by means of a 50 foot shielded coaxial cable. The entire neutron counting system was internally grounded. It was assumed that these precautions prevented any inaccurate readings as a result of radiofrequency interference because no such effects were observed.

CHAPTER III

CALCULATIONS

The efficiency of the NaI(Tl) crystal for 1.332 MeV gamma rays from the decay of cobalt-60 was determined to be 2.60%. A calibrated cobalt-60 button source was used for this determination and its activity was 0.8696 μCi at the time of calibration.

Determination of Thermal and Epithermal Neutron Flux

Indium foil

1.30 MeV (γ) peak in channel 835

16,059 total counts/10 minutes

Covell method for Baseline Subtraction[7]

Left channel = 74 counts

Right channel = 39 counts

$(\dfrac{74 + 39}{2})$ 65 = 16,059 gross counts
− 3,672 background counts
12,387 net counts

Cadmium-covered indium foil

1.30 MeV (γ) peak in channel 830

7,737 total counts/10 minutes

Covell method for Baseline Subtraction

Left channel = 36 counts

Right channel = 127 counts

$(\dfrac{36 + 127}{2})$ 81 = 7,737 gross counts
− 6,601 background counts
1,136 net counts

The values of 12,387 counts and 1,136 counts represent the net measured counts (background corrected) of the indium and cadmium-covered indium foils respectively for the ten minute counting period. To simplify the presentation of the information in the following section, all of the numbers are used without specific indication of inherent statistical counting errors.

To determine the saturation count rate at the end of the activation period, corrections for decay during activation, decay from the end of activation to the beginning of counting and decay during counting must be made.[8] Thus,

Correction of activity during irradiation

$$A_1 = A_o \, (1 - e^{-\lambda ta})$$

Correction of activity due to decay

$$A_2 = A_1 \, e^{-\lambda td}$$

Correction of activity during counting

$$A_3 = (A_2/\lambda tc) \, (1 - e^{-\lambda tc})$$

where:

λ = decay constant of indium-116m $(\lambda = \frac{\ln 2}{54.2 \text{ min}})$

A_o = saturation activity

A_1 = activity after irradiation

A_2 = activity just after decay or just before counting

A_3 = average count rate during counting

ta = activation time (11 minutes)

td = decay time (2 minutes)

tc = counting time (10 minutes)

M = measured number of counts in interval tc.

Either of the following formulas is used to determine the saturation count rate of the foils at the end of the activation period: [2,8,9,10]

$$A_o = A_3 \left[\frac{\lambda tc}{(1 - e^{-\lambda ta}) \, e^{-\lambda td} \, (1 - e^{-\lambda tc})} \right]$$

$$A_o = \left[\frac{\lambda M e^{\lambda td}}{(1 - e^{-\lambda ta}) \, (1 - e^{-\lambda tc})} \right]$$

Thus, the saturation count rates of the indium and cadmium-covered indium foils are 10,316 cpm and 946 cpm respectively. Correcting for a counting efficiency of 2.60% and a branching ratio of 80% yields saturation activities of 8266 dps and 758 dps respectively for the two foils. More accurate results would be obtained were the activation time increased and the counting period shortened. Statistical distribution of the number of counts can seriously affect accuracy if the counting period is too short. Considering the low flux (see calculations) and the relatively long half-life of 54.2 minutes in terms of accelerator operating time, a compensation must be made between operating time and statistical accuracy. Any numerical difference in saturation activity between the two methods of calculation was found to be small and within the accuracy of the counting statistics.

The following formula is used to determine the activity induced by the absorption of thermal neutrons:

$$A_{th} = A_{In} - A_{Cd} + In$$

Thus:

$$A_{th} = 8266 \text{ dps} - 758 \text{ dps}$$

$$A_{th} = 7508 \text{ dps}$$

The thermal neutron flux is given by:

$$\phi_{th} = \frac{A_{th}}{N \, \sigma_{th}}$$

where:

$$\sigma_{th} = 128.5 \times 10^{-24} \text{cm}^2 \quad (\text{Ref. 10})$$

$$N = \frac{(\text{Avogadro's number})(\text{wt. in grams})(\% \text{ abundance})}{\text{Atomic weight}}$$

$$N = \frac{(6.023 \times 10^{23})(0.9537)(0.957)}{114.82}$$

$$N = 4.787 \times 10^{21} \text{ atoms}$$

$$\phi_{th} = 1.22 \times 10^4 \text{n cm}^{-2} \text{sec}^{-1}$$

The cadmium covers are opaque to the neutrons below 0.4 eV in the neutron flux produced during the operation of the accelerator. The cadmium covers are transparent to epithermal neutrons because the large resonance absorption cross-section that exists for cadmium at the upper end of the thermal region falls off rapidly to 10 barns at

the 1.44 eV energy level. Therefore, the induced activity of the cadmium-covered indium foil is essentially due to epithermal neutrons. Thus:

$$\phi_{epithermal} = \frac{A_{Cd + In}}{N \, \bar{\sigma}_{resonance}}$$

where:

$\bar{\sigma}_{resonance}$ = average resonance absorption cross-section for epithermal neutrons by indium

$$= 2550 \times 10^{-24} cm^2 \quad (Ref. 10)$$

$$N = \frac{(6.023 \times 10^{23})(0.9276)(0.957)}{114.82}$$

$$N = 4.656 \times 10^{21} \text{ atoms}$$

$$\phi_{epithermal} = 6.3 \times 10^1 \text{ n cm}^{-2}\text{sec}^{-1}$$

Calculation of the Cadmium Ratio (or degree of thermalization):

cadmium ratio = $\dfrac{\text{indium foil activity-cadmium covered foil activity}}{\text{cadmium covered foil activity}}$

$$= \frac{8266 \text{ dps} - 758 \text{ dps}}{758 \text{ dps}}$$

$$= 9.9 \pm 0.4$$

Determination of Fast Neutron Flux

A maximum dose equivalent rate of 1500 mrem hr^{-1} was measured at the isocenter by the Eberline PNR-4 when the Bonner ball was encased in cadmium (closed collimators, 500 rads min^{-1} for photons).

The 1500 mrem hr^{-1} reading was produced by fast and epithermal neutrons produced during operation of the Clinac-18 linac.

$$\phi_{epithermal} = 63 \ n cm^{-2} sec^{-1}$$

$$\phi_{epithermal \ dose \ equivalent \ rate} = (63 \ n \ cm^{-2} sec^{-1}) \ x$$

$$(\frac{1 \ mrem \ hr^{-1}}{250 \ n \ cm^{-2} sec^{-1}}) = 0.25 \ mrem \ hr^{-1} \quad (Ref. 11, 12)$$

Therefore, most of the measured dose equivalent rate is produced by fast neutrons. For all practical considerations, the dose equivalent rate produced by epithermal neutrons can be ignored because 0.25 mrem hr^{-1} is an insignificant fraction when compared to 1500 mrem hr^{-1}.

Thus,

$$\phi_{fast \ dose \ equivalent \ rate} = 1500 \ mrem \ hr^{-1}$$

$$\phi_{fast} = (1500 \ mrem \ hr^{-1}) \ (\frac{7 \ n \ cm^{-2} sec^{-1}}{1 \ mrem \ hr^{-1}}) \quad (Ref. 11, 12)$$

$$\phi_{fast} = 1.0 \ x \ 10^4 \ n \ cm^{-2} sec^{-1}$$

Calculation of Neutron Fluence per Rad of Photons

(a) Fast neutron fluence per rad of photons = $(1.0 \ x \ 10^4 \ n \ cm^{-2} sec^{-1}) \ x$

$$(60 \ sec \ min^{-1}) \ (11 \ min) = \frac{6.6 \ x \ 10^6 n \ cm^{-2}}{4,995 \ rads}$$

$$= 1.32 \ x \ 10^3 n \ cm^{-2} rad^{-1}$$

(b) Thermal neutron fluence per rad of photons =

$(1.22 \times 10^4 \text{n cm}^{-2}\text{sec}^{-1})$ $(60 \text{ sec min}^{-1})$ (11 min) =

$\dfrac{8.05 \times 10^6 \text{n cm}^{-2}}{4,995 \text{ rads}}$ = $1.61 \times 10^3 \text{n cm}^{-2} \text{ rad}^{-1}$

(c) Epithermal neutron fluence per rad of photons =

$(6.3 \times 10^1 \text{n cm}^{-2}\text{sec}^{-1})$ $(60 \text{ sec min}^{-1})$ (11 min) =

$\dfrac{4.15 \times 10^4 \text{n cm}^{-2}}{4,995 \text{ rads}}$ = $8.32 \text{ n cm}^{-2} \text{ rad}^{-1}$

(d) Total neutron fluence per rad of photons =
Fast + Thermal + Epithermal = $2.93 \times 10^3 \text{n cm}^{-2} \text{ rad}^{-1}$

Calculation of Neutron Dose per Rad of Photons

(a) Fast neutron dose (units) = [rad dose$_{n_{fast}}$ /rad dose$_{photons}$]

$= (1.32 \times 10^3 \text{n cm}^{-2} \text{ rad}^{-1})$ $(3.97 \times 10^{-9} \text{ cm}^2 \text{ rad n}^{-1})$ (Ref.13)

$= 5.24 \times 10^{-6}$ rad dose$_{n_{fast}}$ /rad dose$_{photons}$

--OR--

(b) 4,995 rads/11 minutes = 7.568 rads sec^{-1} for photons

1500 mrem hr^{-1} = 1.5 rem hr^{-1} = 2.5×10^{-2} rem min^{-1} =

4.1×10^{-4} rem sec^{-1} Fast neutron Q.F. = 10 (Ref.14)

Rads x Quality Factor = rem

$\dfrac{4.1 \times 10^{-4} \text{ rem sec}^{-1}}{10}$ = 4.1×10^{-5} rad sec^{-1} for n$_{fast}$

$$(4.1 \times 10^{-5} \text{rad sec}^{-1}) \; (7.568 \text{ rads sec}^{-1}) \; \dfrac{1}{} =$$

$$\underset{n_{fast}}{} \qquad \qquad \underset{photons}{}$$

$$= 5.4 \times 10^{-6} \text{rad dose}_{n_{fast}} \; / \text{rad dose}_{photons}$$

Agreement of calculations in part (a) and (b) above indicates that the conversion factor $(3.97 \times 10^{-9} \text{ cm}^2 \text{ rad n}^{-1})$ is accurate.

(c) Thermal neutron dose (units) = [rad dose$_{n_{th}}$ /rad dose$_{photons}$]

$$= (1.61 \times 10^{3} \text{n cm}^{-2} \text{rad}^{-1}) \; (4.57 \times 10^{-10} \text{n}^{-1} \text{cm}^{2} \text{rad}) \qquad \text{(Ref. 13)}$$

$$= 7.35 \times 10^{-7} \text{rad dose}_{n_{th}} \; / \text{rad dose}_{photons}$$

--OR--

(d) 4,995 rads/11 minutes = 7.568 rads sec^{-1} for photons

$\phi_{thermal}$ dose equivalent rate = $(1.22 \times 10^{4} \text{n cm}^{-2} \text{sec}^{-1}) \times$

$$\dfrac{1 \text{ mrem hr}^{-1}}{300 \text{ n cm}^{-2} \text{sec}^{-1}} \qquad \text{(Ref. 11,12)}$$

$$= 4.0 \times 10^{1} \text{ mrem hr}^{-1} = 6.7 \times 10^{-4} \text{ rem min}^{-1} = 1.1 \times 10^{-5} \text{rem sec}^{-1}$$

Thermal neutron Q.F. = 2.4   (Ref.14)   Rads x Q.F. = Rem

$$\dfrac{1.1 \times 10^{-5} \text{rem sec}^{-1}}{2.4} = 4.7 \times 10^{-6} \text{rad sec}^{-1}$$

$$(4.7 \times 10^{-6} \text{rad sec}^{-1}) \; (7.568 \text{ rads sec}^{-1}) \; \dfrac{1}{} = 6.2 \times 10^{-7} \text{ rad dose}_{n_{th}} /$$

rad dose$_{photons}$

The results of calculations in part (c) and (d) above are in good agreement.

(e) Epithermal neutron dose (units) = [rad dose$_{n_{epi}}$ /rad dose$_{photons}$]

4,995 rads/11 minutes = 7.568 rads sec^{-1} for photons

$\phi_{epithermal}$ dose equivalent rate = (63 n cm^{-2}sec^{-1}) ($\dfrac{1 \text{ mrem hr}^{-1}}{250 \text{ n cm}^{-2}\text{sec}^{-1}}$)

(Ref. 11,12)

= 2.5 x 10^{-1} mrem hr^{-1} = 4.2 x 10^{-6} rem min^{-1} = 7.0 x 10^{-8} rem sec^{-1}

Epithermal neutron Q.F. = 2 (Ref.14)   Rads x Q.F. = Rem

Epithermal neutrons $=$ neutrons of energies of about 1 eV to 10 keV. (Ref. 19)

$\dfrac{7.2 \times 10^{-8} \text{rem sec}^{-1}}{2}$ = 3.6 x 10^{-8}rad sec^{-1}

(3.6 x 10^{-8}rad sec^{-1}) ($\dfrac{1}{7.568 \text{ rads sec}^{-1}}$) =

4.7 x 10^{-9} rad dose$_{n_{epi}}$ /rad dose$_{photons}$

Percent Neutron Dose Equivalent Compared to Photon Dose Equivalent
   (per minute)

(a) Fast neutron dose equivalent rate   = 2.5 x 10^{-2}rem min^{-1}

Thermal neutron dose equivalent rate   = 0.067 x 10^{-2}rem min^{-1}

Epithermal neutron dose equivalent rate = 0.00042 x 10^{-2}rem min^{-1}
                                                         +
──
Total neutron dose equivalent rate   = 2.56 x 10^{-2}rem min^{-1}

The thermal and epithermal neutron contribution to the total neutron dose equivalent rate is insignificant.

10 MV photons = 10 MeV photon energy average

Q.F. for 10 MeV photons = 1 (Ref. 14, 15, 16)

500 rads (10 MV photons) = 500 rem

$$\frac{2.5 \times 10^{-2} \text{rem min}^{-1}}{500 \text{ rem min}^{-1}} \times 100 = 5 \times 10^{-3}\%$$

Total Neutron Dose Equivalent to Patient Receiving 5000 rads of Photons

Total neutron dose equivalent rate = 2.5×10^{-2} rem min^{-1}

Time necessary to deliver 5,000 rads of photons = 10 minutes

$(2.5 \times 10^{-2}$ rem min$^{-1})$ (10 min) = 0.25 rem total

Total Neutron Dose to Patient Receiving 5,000 rads of Photons

Fast neutron dose rate = 2.5×10^{-3} rad min^{-1}

Thermal neutron dose rate = 0.28×10^{-3} rad min^{-1}

Epithermal neutron dose rate = 0.0021×10^{-3} rad min^{-1}
                                    +
_____

Total neutron dose rate = 2.7×10^{-3} rad min^{-1}

The epithermal neutron contribution to the total neutron dose rate is insignificant.

$(2.7 \times 10^{-3}$ rad min$^{-1})$ (10 min) = 2.7×10^{-2} rad

Percent Neutron Dose Compared to Photon Dose (per minute)

$$\frac{2.7 \times 10^{-3} \text{rad min}^{-1}}{500 \text{ rad min}^{-1}} \times 100 = 5.4 \times 10^{-4}\%$$

CHAPTER IV

DISCUSSION

Throughout the entire neutron measurements experiment, an approach was used to produce a conservative estimate of the patient neutron exposure. An effort was made to maximize the production of neutrons and the resulting values obtained. Thus, this approach was somewhat different than that usually found in the literature. A major departure in methodology involved the closure of the tungsten collimators, which expectedly increased the production of neutrons. This technique was used to make a comparison of the neutron dose (equivalent) with the collimators closed to the photon dose (equivalent) with the collimators open at the isocenter. The neutron energy spectrum was not affected because tungsten is a very poor neutron thermalizer. Since tungsten is a high density, high atomic number element, neutrons interact principally through inelastic collisions. Also, the closure of the collimators shielded the cadmium disks and indium foils from photoneutron interference. The design specifications require less than 0.5% photon leakage through the collimators. This means that the indium foils were activated mostly by neutrons. Since the absorption cross-section of indium is well defined for thermal neutrons, the thermal flux calculated from indium foil activation should be a good value. The epithermal flux is very low, based on the low counts obtained from the cadmium covered indium foil by the NaI(Tl) counting system. The exact value of the epithermal flux will of course depend upon the value of the resonance absorption cross-section selected. Some investigators prefer to report their results

24

in terms of neutrons per square centimeter for an irradiation because
the flux derived from foil activations is an averaged value for the
irradiation time.

The shape of the Clinac-18 photoneutron energy spectrum is
unknown at this time.[2] Therefore, the fast neutron flux cannot be
measured accurately. The best assumption that can be made is that
the Clinac-18 photoneutron energy spectrum is not too dissimilar from
a fission neutron energy spectrum with an average energy of about
1.5 MeV. This assumption is based on information provided by the
National Bureau of Standards.[20]

The Clinac-18 photoneutron energy spectrum can be determined
with a neutron spectrometer. If such equipment is not available,
an approximation of the shape of the spectrum can be made with
threshold detectors. None of these instruments were available to
this investigator. The fast neutron flux is so low with the limit
protected Clinac-18 (1,000 rads min^{-1} photons maximum) the threshold
foil technique would be marginally successful.

A series of threshold detectors can be used to determine the
flux in each of a series of energy intervals.[17] The total flux of
all energies above 1 keV is first measured by determining the rate
of fission induced in a plutonium-239 activation foil shielded by
boron-10. In this manner the absorption cross-section of plutonium-
239 is approximately constant for all energies down to 1 keV. Next,
the rate of fission induced in a neptunium-237 foil is determined.
The threshold for this reaction is 0.7 MeV. The difference between
the two measurements determines the flux in the interval 1 keV-0.7

MeV. Measurement of the fission rate induced in a uranium-238 foil (1.5 MeV threshold) compared to that of the neptunium-237 foil determines the flux in the 0.7 MeV-1.5 MeV interval. Comparison of the fission rate induced in the uranium-238 foil with the (n, p) reaction in sulphur-32 (threshold 2.5 MeV) determines the fluxes in the energy intervals of 1.5 MeV-2.5 MeV and above 2.5 MeV. A histogram of the neutron energy spectrum can be constructed from this information. Proton recoil in the $^{32}S(n, p)^{32}P$ reaction can be used to determine the reaction rate as well as measurement of the β^- intensity (with liquid scintillation technique) from the decay of phosphorous-32.[18]

Fast neutron flux cannot be measured as precisely as thermal neutron flux.[19] The cross-section of a threshold monitor varies over a wide range of energies. Therefore, no single cross-section can accurately characterize the fast neutron flux. The fast flux can only be approximated by using average cross-sections. Thus, if the average cross-section is known for one or more threshold detectors, the fast flux can be measured.

During patient treatment with the Clinac-18, the patient's exposure to neutrons is essentially whole-body. Speculation would lead one to expect the shape of the Clinac-18 fast neutron energy spectrum to vary with position. Therefore, threshold monitoring techniques or future neutron spectrometric analysis should investigate this possibility. This point is important because most of the neutron dose is from fast neutrons.

The Eberline PNR-4 neutron detector and Bonner ball survey instrument was used for neutron dosimetry in this investigation. It was calibrated for use with a californium-252 neutron fission spectrum. The accuracy of the measurements obtained from its use do not include any possible errors as a result of variation in response of the detector with neutron energy. Also, the pulsing nature of the radiation produced by the Clinac-18 linac can be ignored for the PNR-4 measurements because the resolving time of the neutron detector was not sufficiently short to detect such pulsing. The PNR-4 did not show any increase in field strength with time. Therefore, it can be assumed that there was no appreciable build-up of charge within the detector. This fact means the dose equivalent rate indicated is a true time-averaged rate and can be used as if neutron production were continuous.

It was experimentally determined that the total neutron dose equivalent rate is a function of two parameters. The neutron dose equivalent rate increases linearly with increased photon dose rate and also increases with decreasing field size or increasing collimator material in the beam (See Figure II-2). The total neutron dose equivalent rate was observed to decrease by 80% when the collimators were opened versus closed. This seems to indicate that 80% of the photoneutrons are produced by (γ, n) reactions in the tungsten collimators. Figure II-3 is a second generation graph which can be consulted to determine the total neutron dose equivalent rate at the isocenter produced by any combination of photon dose rate and square field-size setting.

CHAPTER V

CONCLUSIONS

1. The neutron dose at the isocenter produced by thermal, epithermal
   and fast neutrons has a maximum total value of 5.4×10^{-4}%
   of the photon dose with the collimators closed. The neutron
   dose equivalent under the same conditions is 5×10^{-3}% of
   the photon dose equivalent.

2. The cadmium ratio is approximately ten when the collimators are
   closed. This value indicates a moderate degree of
   thermalization of the neutron flux.

3. The neutron dose to the cancer patient is insignificant and can
   be ignored.

4. The Clinac-18 linac is an inefficient neutron generator.

5. Shielding of Clinac-18 linac facilities should include consideration
   of neutron production but it is generally more than adequate
   if the photon protection is adequate.

6. The production of neutrons during operation of the Clinac-18
   linac is a function of collimation and photon dose rate.
   Both neutron dose and dose equivalent decrease as the
   collimators are opened. Both neutron dose and neutron dose
   equivalent decrease linearly as the photon dose rate is
   decreased.

REFERENCES

1. Adapted from the Varian Clinac-18 ® service manual by Varian Associates of Palo Alto, California.

2. McGinley, P. H., et al. Journal of Medical Physics, Vol. 3 No. 6, Nov./Dec. 1976.

3. Deye, J. A. and F. C. Young. Journal of Physics in Medicine and Biology, Vol. 22, No. 1, p. 90-94. 1977.

4. Law, J. and F. A. Iddings. Journal of Radioanalytical Chemistry, Vol. 3, p. 53-63, 1969.

5. Berman, B. L. Atlas of Photoneutron Cross-Sections Obtained with Monoenergetic Photons. U. S. AEC Rep. URCL-75694 (1974).

6. Tapley, N., M. D. editor - "Clinical Applications of the Electron Beam". Chapter Two," Radiation Physics of Electron Beams" by Peter R. Almond, Ph.D., p. 7-80. Published by John Wiley & Sons, Copyrighted 1976.

7. Covell, D. F. "D. F. Covell Method", Journal of Analytical Chem. 31:1785-1790, 1959.

8. Profio, A. E. "Experimental Reactor Physics," by John Wiley and Sons, copyright 1976.

9. Daavettila, D. A., et al. "A Manual of Reactor Laboratory Experiments," Argonne National Laboratory, Jan. 1965. ANL-6990, p. 27.25, 28.21.

10. -, "Neutron Activation Foils-- Research Foils," unpublished report prepared by the scientific staff of Reactor Experiments, Inc. San Carlos, California (Circa 1972).

11. Stevenson, G. R., et al. "Standardizing the Fluence - to - Dose - Equivalent Conversion Factors for Whole - body Neutron Exposures," in Neutron Monitoring for Radiation Protection Purposes, Vol, I, Proceedings of a Symposium on Neutron Monitoring for Radiation Protection Purposes. Session II, p. 177-191. Published by the International Atomic Energy Agency, Vienna, 1973.

12. Rockwell, T. editor. "Reactor Shielding Design Manual," published by Van Nostrand, Princeton, New Jersey. copyright 1956.

13. Stoddard, D. H. and H. E. Hootman. Cf-252 Shielding Guide, U. S. AEC Rep. DP-1246 (1971).

14. Courtney, J. C., editor. "A Handbook of Radiation Shielding Data".
    Sponsored by the Nuclear Science Center, Louisiana State
    University (Baton Rouge) and the Shielding and Dosimetry
    Division of the American Nuclear Society. Distributed by
    LSU Bookstore, Union Building, Baton Rouge, LA 70893.

15. Morgan, K. Z. and J. E. Turner, editors. "Principles of Radiation
    Protection", by John Wiley and Sons, New York. Copyright
    1967.

16. Recommendations of the International Commission on Radiological
    Protection, ICRP Publication 4, Report of Committee IV
    (1953-1959) on "Protection Against Electromagnetic Radiation
    Above 3 MeV and Electrons, Neutrons and Protons," the
    MacMillan Company, New York, 1964.

17. Whyte, G. N. "Principles of Radiation Dosimetry," by John Wiley
    and Sons, New York. Copyright 1959.

18. Greene, T. A. A thesis submitted to the Graduate Faculty of
    the Louisiana State University and Agricultural, and
    Mechanical College. May 1974.

19. Lyon, W. S., Jr., editor. "Guide to Activation Analysis" prepared
    by Division of Isotopes Development, U.S.A.E.C. Published
    and prepared under Auspices of the Division of Technical
    Information, U.S.A.E.C., Published by D. Van Nostrand Company,
    Inc., Princeton, New Jersey. Copyright 1964.

20. U.S. National Bureau of Standards, Handbook 97. "Shielding for
    High-energy Electron Accelerator Installations," p. 25,
    1964.

VITA

Grayson Scott Young, Jr. was born on May 25, 1949, in Baton Rouge, Louisiana. He attended Broadmoor High School in Baton Rouge, Louisiana and graduated in May, 1967.

In May, 1967 he entered Louisiana State University and graduated with a Bachelor of Science degree in General Studies in May, 1974. He held numerous jobs throughout his undergraduate college experience.

He entered graduate school in Nuclear Engineering at LSU in August, 1975. At that time, he received a graduate assistantship in the Nuclear Science Center. He worked in the area of student laboratory instruction with various professors. He was treasurer of the LSU student chapter of the American Nuclear Society from September 1977 to July 1978.

He is presently a candidate for the degree of Master of Science in the Department of Nuclear Engineering.

EXAMINATION AND THESIS REPORT

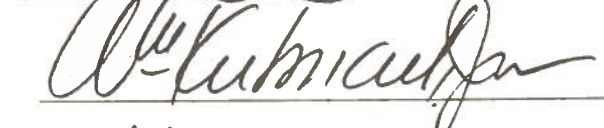Candidate: Grayson Scott Young, Jr.

Major Field: Nuclear Engineering

Title of Thesis: Evaluation of the Output from a Bent-beam Medical Linear Accelerator

Approved:

Frank A. Iddings
Major Professor and Chairman

_____
Dean of the Graduate School

EXAMINING COMMITTEE:

Edward D. Lambremont

Wm. Cubriault Jr.

Ralph C. McIlhenny

_____

_____

_____

Date of Examination:

July 14, 1978